Photoelectron-initiated avalanches in low-pressure glow discharges

Annette Mitchell, Geoffrey R. Scheller, and Richard A. Gottscho
AT&T Bell Laboratories, Murray Hill, New Jersey 07974

David B. Graves
Chemical Engineering Department, University of California, Berkeley, Berkeley, California 94720
(Received 21 April 1989)

Photoelectron-initiated avalanches can be used to enhance ionization and dissociation, monitor surface properties, and test models of low-pressure glow discharges. In this work we explore the effects that discharge power and frequency have on electron avalanching and find that lower-powered discharges exhibit inherently larger gain. Transient changes in both current (optogalvanic effect) and optical emission intensity are enhanced three- to fivefold relative to higher-powered discharges. Monte Carlo simulations show that sheath thickness, and not voltage, is the primary parameter that determines the extent of avalanching and current gain. A self-consistent single-beam fluid model shows that optogalvanic oscillations are produced by overcompensation of the plasma potential in releasing excess negative charge produced by photoemission at the cathode. The beam model is in good qualitative but only fair quantitative agreement with experimental observations because of implicit assumptions about electron scattering. Multibeam and hybrid particle-fluid codes should provide a better quantitative description. For materials-processing applications these results imply that photoinitiated avalanches are best used in enhancing low-powered discharges. Similarly, reactive surfaces are most sensitively monitored *in situ* using optogalvanic detection of photoemitted electrons in weak discharges. We also find the photoelectric yield sensitive to discharge frequency when photon energies near the excitation threshold are used. This effect is attributed to surface charging that shifts the photoelectric threshold energy.

I. INTRODUCTION

Recently, photoelectron emission has been used in low-pressure plasma materials processing for enhancing the degree of ionization and dissociation in the discharge[1] and for monitoring the condition of reactive surfaces.[2,3] By using photoelectric emission to enhance ionization and dissociation, discharges can be operated at lower voltages and pressures. In etching applications, for example, photoemission-enhanced discharges could be used to minimize ion-induced damage without sacrificing anisotropy and rate. Photoelectric emission can also be used to monitor process endpoints and surface contamination. For example, when thin films of SiO_2 on Si are etched in fluorine-containing plasmas, a large increase in discharge current (optogalvanic effect) is observed when the oxide clears and the underlying Si is exposed.[2,3] If the photon energy is near the Si photoelectric threshold, the signal rapidly decreases with further exposure to the reactive plasma because fluoride contamination of the surface produces a work function shift that results in a decrease in photoelectric yield.

Electron emission from electrode surfaces is also important from a fundamental discharge physics point of view. For example, cold cathode dc discharges can only be self-maintained by secondary-electron emission from the electrodes. Similarly, the γ regime of radio-frequency (rf) glow discharges is characterized by intense secondary-electron emission.[4] Thus, it is of interest to understand the avalanche that occurs when an electron is released from the cathode of low-pressure glow discharges.

In this work we trigger an avalanche of electrons by using a short-pulsed laser to stimulate photoelectron emission from the cathode of abnormal dc and rf glow discharges. The effects of the electron avalanche are monitored by detecting both the photoemission optogalvanic (POG) signal and the transient change in optical emission intensity. Optical monitoring of photoelectron emission has been used previously to study transport properties of electrons in weak, uniform electric fields[5] and more recently in strong, uniform electric fields.[6] The optogalvanic effect and concomitant changes in sheath fields of rf discharges caused by the similar process of gas-phase photodetachment has also been reported recently.[7] Here, the short-time changes in current and optical emission resulting from release of electrons from the cathode into the strong, nonuniform cathode fall electric field are monitored and modeled. This work differs from the following companion work by Debontride *et al.* in that[8] (1) the range of discharge power densities is nearly 100-fold larger in this work. Thus, all the results in Ref. 8 correspond to the low-power regime of this work and the power dependence is insignificant. (2) The pulse duration of the photoemission source in this work is nearly tenfold shorter than in the companion work. Thus, the ringing observed in this work is less evident in Ref. 8. The following paper also presents detailed, *in situ* elec-

tric field measurements of the discharge response to the photo-initiated avalanche. Other differences are as enumerated in Ref. 8.

In part, this work is motivated by the need to optimize POG signals for sensitive *in situ* surface monitoring. It is also desirable to understand under what conditions discharges can be significantly intensified to increase degrees of ionization and dissociation for materials processing applications.[1] Finally, the experiments are used to test the self-consistent single-electron beam model that has been found to work well in describing the steady-state properties of dc and rf glow discharges.[9–11]

We find that the optogalvanic signal depends strongly on steady-state discharge power. The *absolute* intensities of both the optogalvanic and transient optical emission signals are 3–5 times larger at low power than at high power. Although the cathode fall voltage is smaller, the thicker sheath in the lower-powered discharge leads to more avalanching. The validity of this hypothesis is supported using Monte Carlo simulations for fixed field profiles. For a self-consistent description, we turn to a simple model that treats avalanching electrons as a monoenergetic, unidirectional beam; however, this single-beam model is in only fair quantitative agreement with experiment. Nonetheless, qualitative trends are reproduced in the simulations and physical insight is gained.

When wavelengths near the photoemission threshold are used, we find that the POG signal depends strongly on discharge operating frequency. However, this effect is not attributed to the inherent properties of the discharge but rather to surface charging. In dc discharges, charging is more extensive, the photoelectric threshold shifts to lower energy, and the yield is enhanced relative to rf discharges.

In the sections that follow, we first outline experimental procedures and then discuss observations along with simulation results. Details of the modeling approaches are given elsewhere.[10–12]

II. EXPERIMENTAL PROCEDURE

A. Optogalvanic detection

The POG experiment has been described in detail previously.[2] Briefly, a transient change in discharge current is induced from Al water-cooled cathodes using an excimer laser operating at 248 nm. The signal is recorded with a Tektronix 7912 transient digitizer by measuring the voltage drop across a 50-Ω resistor. The time resolution of the system is dictated primarily by the excimer laser pulse width (~ 10 ns). The unpolarized laser beam is incident at ~70° with respect to the surface normal and allowed to diverge sufficiently to completely cover the electrode surface.

Measurements are made using a configuration of resistors and capacitors as shown in Fig. 1. Neither the magnitudes nor the shapes of the transient current depend significantly on slight modifications of this configuration. For example, the transient current can be monitored at either of the positions indicated in Fig. 1 with both or with only one 50-Ω resistor to ground in the circuit. Typical current transients are shown in Fig. 2. Note that the short time scale over which the current is recorded precludes contributions from ion motion. Within our signal-to-noise limitations, the ion current is not detected when a longer time scale is examined. In the following

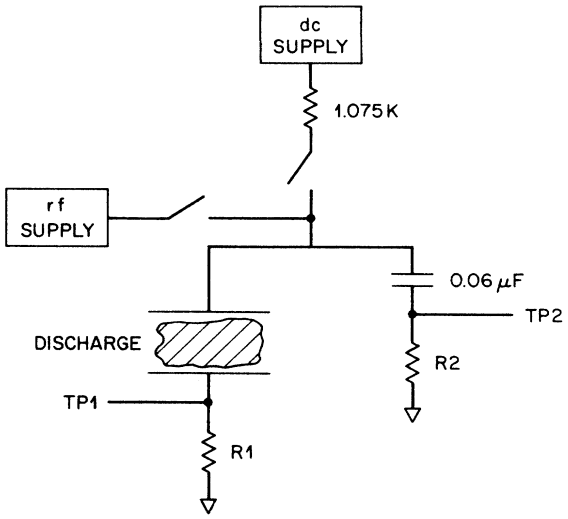

FIG. 1. Typical circuit used to detect optogalvanic signals resulting from photoelectric emission at the cathode. The signal can be sampled from either TP1 or TP2 with the resistors R1 and R2 either 0 or 50 Ω.

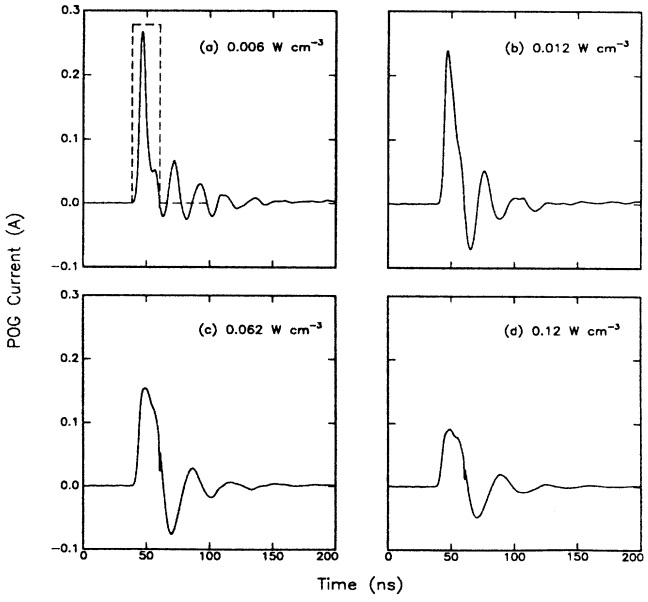

FIG. 2. Photoemission optogalvanic signals as a funtion of time and discharge power. Note the larger signals and increased ringing at lower power. The dashed line in (a) illustrates the placement and width of the current integrating gate used in obtaining the data shown in Fig. 6.

work, enhanced signal-to-noise ratios resulting from higher duty cycle and longer pulse length permit these changes to be observed.

In every case, the POG signals shown in Fig. 2 exhibit ringing in the current waveform that is stronger for lower-powered than for higher-powered discharges. Voltage perturbations are kept to less than $3\pm2\%$ by using the parallel capacitor to ground; a typical voltage waveform is shown in Fig. 3. Care is also taken to ensure that the transient current is linearly dependent on photon flux for constant plasma conditions. At higher photon fluxes, the transient current saturates owing to space-charge limitations and the voltage waveform is significantly perturbed ($\geq 10\%$).[2]

For the data presented in Sec. II B the magnitude of the POG signal is determined by integrating the current waveform using a Stanford Research Systems gated integrator. A 20-ns gate width is used and is synchronized with the firing of the laser using a fast photodiode (EG&G FND-100). The leading edge of the integrating gate is adjusted to coincide with the rising edge of the POG signal [Fig. 2(a)].

Most of the experiments are performed using dc discharges. For rf discharges (250 kHz) the firing of the laser and the opening of the gate are adjusted to coincide with the voltage minimum in the rf cycle.[13] Thus, photoemission is induced from the momentary cathode and the experiments are pseudo-dc.

For all the work presented here, the electrode gap is 4 cm, electrode diameter is 5.08 cm, Ar gas flow rate is 10 sccm (4.46×10^{-4} mol min^{-1}), and pressure is 1.0 Torr. The gas temperature is measured to be 350 K as described previously.[14] No dependence of gas-phase temperature on position in the discharge is observed. Note that similar results are obtained but not presented here when stainless-steel and Si electrodes are used, when He is used instead of Ar, and when the discharge is operated at 0.3 Torr instead of 1.0 Torr. In particular, the changes in POG signal with discharge power and frequency are qualitatively independent of these operating variables.

One difficulty in these experiments, and yet one reason why this technique should be useful for process monitoring, is the variability of the photon-induced electron emission coefficient γ_p. For constant photon flux, the POG current varies slowly over long periods of time (minutes to hours). As appropriate, the laser flux is adjusted to maintain a constant signal level under a specific set of conditions; a range of approximately 2–50 μJ/cm^2 is used. When the laser flux is so adjusted, reproducible trends in POG signal versus frequency and power are achieved. Thus, by monitoring the laser power required to obtain constant POG signal, a measure of the electrode surface emissive properties in materials processing environments could be obtained.

B. Transient emission detection

In addition to monitoring transient current signals, we also measure transient changes in Ar optical emission intensity that result from injection of electrons into the discharge. A $\frac{1}{3}$-m monochromator (Heath EU-700), equipped with an 1180 groove/mm grating blazed at 500 nm and RCA C31034A photomultiplier tube, is used to record the intensity of Ar atom emission lines at 750.4, 603.3, and 811.5 nm as a function of both position and time. Only 750.4-nm emission intensities are shown here but similar results are obtained for the other transitions. The optical setup has been described in detail previously.[15]

For optical emission, the time resolution is limited by photomultiplier and excited-state radiative decay time constants. Therefore, the intensity as a function of time is independent of position in the discharge and propagation of the electron avalanche *appears* to be instantaneous. A typical emission transient is shown in Fig. 4 along

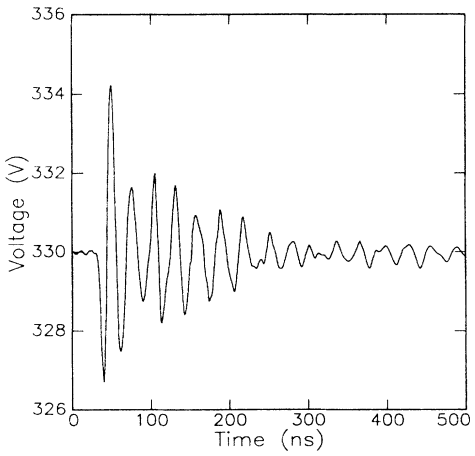

FIG. 3. Typical voltage waveform showing ~2% perturbation due to photoemission.

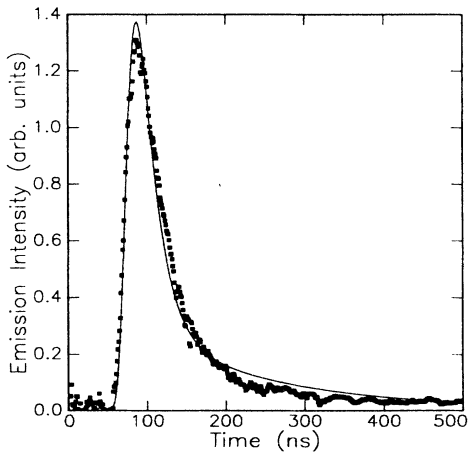

FIG. 4. Ar atom emission at 750.4 nm and 3 mm from the cathode as a function of time. The line is a least-squares fit to the data where only the branching ratio to the $3s'_1$ and $2p_1$ states is varied. Within the experimental time resolution, the excitation avalanche appears instantaneous; the emission decay shown here does not depend on the position from the cathode.

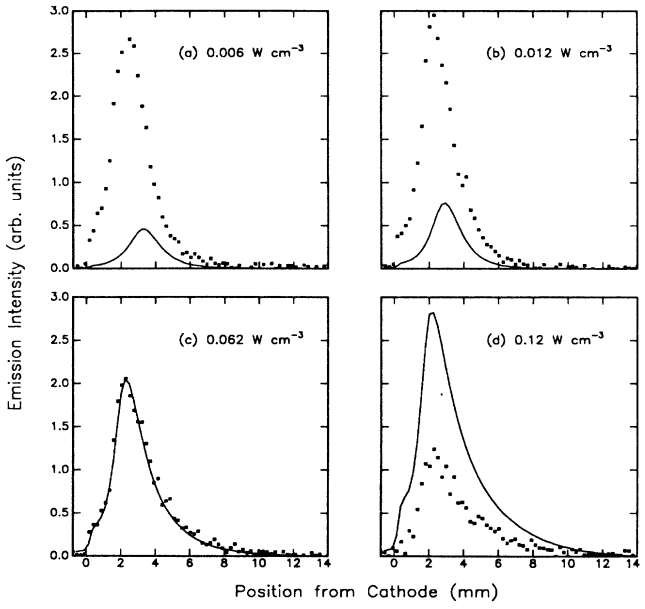

FIG. 5. Ar atom emission spatial profiles as a function of discharge power for both steady-state dc (solid lines) and transient photoemission (points). The steady-state emission profile is normalized to the transient profile in (c); however, for different power densities, the relative emission intensities are as shown. Note the similarity in shapes between the two profiles at higher power and the transient decrease in sheath thickness at lower power. The transient emission intensity is acquired using gated electronic detection and is much larger than the steady-state emission intensity during the gating period; the steady-state emission is acquired using an electrometer and is much larger than the time-averaged transient emission intensity.

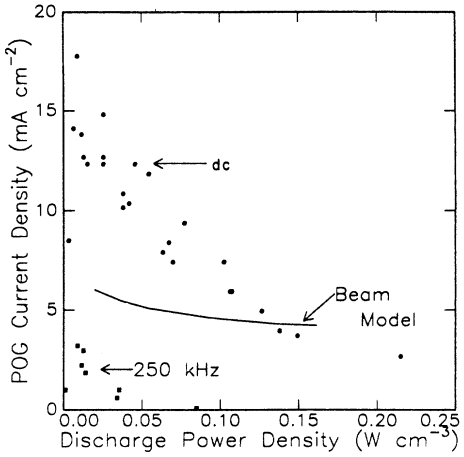

FIG. 6. Dependence of POG signal magnitudes on discharge power for both dc and 250 kHz discharges through Ar. The steady-state current has been subtracted off. Also shown are the results of single-beam model calculations (solid line) for the dc discharge.

with a fit to a simple model that includes cascading from the $3s'_1$ state to the $2p_1$ state (detected by emission into the $1s_2$ state at 750.4 nm) (Paschen notation). Only the initial branching ratio into the $3s'_1$ and $2p_1$ states is varied to fit the data. We find $k'/k \approx 0.8$, where k' and k are electron-impact excitation rates into the $3s'_1$ and $2p_1$ states, respectively. Also included in the model without adjustable parameters is the time response of the detection system (determined by comparing the laser light pulse measured through the monochromator system with that measured independently using a fast photodiode).[16] To determine the emission intensity spatial profile, the time-dependent signal is integrated using a 200-ns gate on the SRS integrator. Typical spatial profiles are shown in Fig. 5 for both transient emission and the steady-state glow.

III. RESULTS

A. POG signal dependence on discharge power

As shown in Figs. 2 and 6, the magnitude of the POG signal depends strongly on discharge power. As the discharge power is increased, the POG signal rapidly decreases. This trend is independent of cathode material, gas composition, and pressure and does not appear to result from changes in γ_p. The effect is observed regardless of the sequence in which the measurements are taken; and, as power is adjusted, no slow transients characteristic of changes in surface properties are evident. For example, if the discharge is run at high power for some time and then changed rapidly to low power, the POG signal immediately increases. Similarly, if this sequence is reversed, the POG signal decreases. In either case, no inhibition period ($\gtrsim 0.5$ s) is evident, suggesting that the change in signal amplitude results from a change in the discharge structure and overall circuit response and not from changes in γ_p. As we now show, this hypothesis is supported by spatially resolved optical emission intensity measurements.

B. Spatial dependence of photoelectric beam current

By examining optical emission from Ar atoms synchronously with the emission of photoelectrons from the cathode, the spatial profile of the electron avalanche is monitored (Fig. 5). Also plotted in Fig. 5 are the steady-state emission spatial profiles. Note the opposite power dependence: *While the steady-state emission intensity increases with discharge power, the transient emission intensity decreases with power.* Under steady-state conditions, the total current is limited by the ion flux to the surface. As the voltage is increased to increase the power, the current and emission intensity increases (Figs. 5 and 7). The sheath roughly corresponds to the spatial region between the cathode and peak emission intensity positions. As seen from emission spatial profiles, this region is thinner at higher power. For a given voltage, a thinner sheath implies a larger charge density.

The decrease in transient emission intensity with power is proportional to the decrease in POG signal as plotted

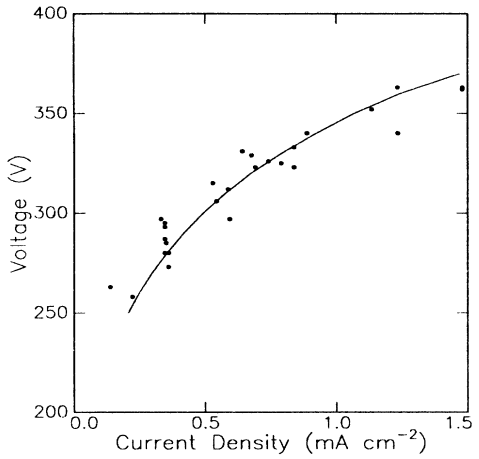

FIG. 7. Current-voltage characteristic for dc discharge through Ar (points). Also shown are single-beam model calculated currents (solid line) for fixed secondary emission coefficient ($\gamma_i = 0.0625$).

in Figs. 2 and 6. For high steady-state power, the transient emission profile coincides with the steady-state, negative-glow profile [Figs. 5(c) and 5(d)]. This observation is consistent with the idea that the dc glow is maintained by a flux of secondary electrons induced by ion impact on the cathode surface. It is also consistent with minimal perturbation of the discharge structure by the excess electron flux.

At low steady-state power, on the other hand, the two profiles no longer coincide. While the transient emission profile still peaks ~2 mm from the cathode as in the high-power discharge, the steady-state profile peaks farther from the cathode at ~3.5 mm. When the electron flux at the cathode in the low-power discharge is increased by photoemission, a major perturbation of the discharge structure occurs and the sheath contracts to a point reminiscent of the high-power discharge (Fig. 5). Note that the sheath contraction implies a displacement current component to the POG signal (see below and the following paper). Along with *in situ* local-field measurements, similar observations have been recorded when the sheath is perturbed by releasing electrons by photodetachment instead of photoemission.[7] Note that the low-power regime explored in the companion paper is between 0 and ~0.03 W cm^{-2} where we do not observe a significant dependence of POG signal on discharge power (Fig. 6).

From the observations above, it appears that the lower-powered discharge has more inherent gain than the high-powered discharge. That is, both photo-enhanced current and emission are increased more at low- than at high-discharge power. Although the sheath voltage is smaller at low power (Fig. 7), the sheath is thicker (Fig. 5); and, the change in sheath thickness appears to be more important than the change in voltage. This is because the gain is created by electron avalanching that occurs primarily in the sheath. Therefore, for similar voltages, the thicker the sheath, the larger the gain.

A significant test for self-consistent discharge models is the accurate simulation of these transient effects. Before proceeding with such a test for the single-beam model, it is useful to examine the output of Monte Carlo simulations of electron avalanching for fixed sheath thickness and voltage drop.

C. Monte Carlo simulations of electron avalanching in the cathode fall

We use a program and approach developed by Boeuf and Marode[12] in simulating avalanching in the cathode fall of He discharges. Cross sections for momentum transfer, excitation, and ionization are taken from Refs. 17–19. For inelastic collisions, scattering is assumed to be isotropic in the center of mass; for ionization collisions, 10% of the available energy is given to the secondary electron. All electrons, including progeny, are tracked for each of 10 "seed" electrons originating at the cathode surface with an initial energy of 1 eV. Because all electrons are followed, the calculations are time consuming when the gap is large and the sheath is small because slow electrons vastly outnumber fast electrons. Therefore, simulations are done for gaps smaller than the experimental value of 4 cm. We find no qualitative differences when the results from 1- and 2-cm gap simulations are compared. Similarly, if we increase the number of seed electrons from 10 to 20, the qualitative results remain unchanged. For further details see Ref. 12.

The reader will note that the simulation described above differs from experiment in the gap and gas composition. Note also that the effects of photon- and metastable-induced secondary-electron emission are not considered. Therefore, the model is useful merely to

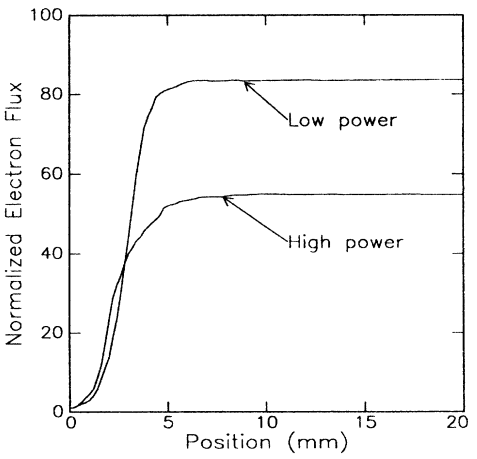

FIG. 8. Total electron flux normalized to initial flux calculated using Boeuf and Marode's Monte Carlo code for linear electric fields. For the solid line, the cathode fall voltage and sheath thickness are 275 V and 3.5 mm, respectively. For the dashed line, 370 V and 2.0 mm. Note that the larger gain for the lower voltage and thicker sheath corresponding to the lower-powered discharge. As discussed in the text, a gap of 20 mm is chosen to minimize computational time.

show trends; quantitative aspects of the avalanche cannot be compared meaningfully to experiment.

The results from two simulations are shown in Fig. 8. In the first, the voltage and sheath thickness are set to 275 V and 3.5 mm, respectively. These conditions correspond to the low-power discharge (~ 0.012 W cm^{-3}). The second simulation is done for 370 V and 2.0 mm, corresponding to the high-power discharge (~ 0.12 W cm^{-3}). Clearly the electron flux reaches a larger value for the thicker sheath and lower voltage confirming the idea that the lower-powered discharge has inherently higher gain.

D. Single-beam model

Although Monte Carlo simulations are useful for characterizing the extent of avalanching, the calculations as employed here are not self-consistent. Neither the ion flux nor changes in the electric field are considered. On the other hand, it is difficult and time consuming to simulate the discharge in full detail with a self-consistent model. Therefore, we turn to a simpler, albeit less accurate, description that self-consistently accounts for changes in sheath fields.

A recent approach to self-consistent discharge simulation is solving Poisson's equation simultaneously with equations of continuity for ions and bulk electrons. A second group of fast electrons, the so-called beam electrons, resulting from secondary emission induced by both ions and photons at the cathode surface, are described by separate continuity and energy-balance equations.[9,10] The beam is assumed to be unidirectional and monoenergetic. While clearly a crude approximation, this model has been found to work well in describing the properties of uniform E/N electric field to density ratio, Townsend discharges and steady-state abnormal dc and rf glows.[9-11]

$$\Gamma_b = \gamma_p \Gamma_p + \gamma_i \Gamma_i \ , \tag{1a}$$

where the Γ's are fluxes (cm^{-2}s^{-1}) and the γ's are (unitless) electron emission coefficients. The photon flux is expressed as a function of time according to

$$\Gamma_p(t) = \Gamma_p \exp[-(t-t_0)^2/\tau] \tag{1b}$$

where $\tau = 6\times 10^{-9}$ s corresponds to Gaussian full width at half maximum (FWHM) of 10 ns. The product of $\gamma_p \Gamma_p = 1.7\times 10^{16}$ cm^{-2}s^{-1} corresponds to a peak transient beam current density at the cathode of $\Gamma_b = 2.7$ mA cm^{-2} and is chosen to match the experimentally observed optogalvanic signal ≈ 4.3 mA cm^{-2} at 0.13 W cm^{-3} (370 V, 1.48 mA cm^{-2}). For a peak laser intensity of 1 kW cm^{-2}, this product corresponds to $\gamma_p = 1.4\times 10^{-5}$, which is not an unreasonable number for oxidized Al near threshold. We operationally define gain to be the ratio of the transient current to the steady-state current and from the data in Figs. 6 and 7, we see that the gain ranges from ~ 2 at high power to ~ 75 at low power.

A uniform mesh of 400 points is used. Boundary conditions are placed on ion and electron densities and fluxes as described in Ref. 11. The beam energy is set equal to 0.1 eV as discussed previously.[11] γ_i is fixed at 0.0625 and good agreement between experiment and theoretical current-voltage characteristics is obtained (Fig. 7). Note that γ_i and $\gamma_p \Gamma_p$ are the only free parameters in the steady-state and transient simulations, respectively. They are chosen to match one set of experimental data and then fixed thereafter. The voltage boundary condition is set equal to the applied voltage and the small variation caused by photoemission is ignored. Although inconsistent with experiment, this assumption permits us to evaluate the extent of ringing inherent in the discharge independently of interactions with the external circuit. We will also explore briefly the consequences of nonconstant voltage.

Note that although the emission data suggest that the beam propagation is instantaneous, it is still necessary to simulate the beam using the fully time-dependent equations.[11] If the beam time dependence is not included, the current is not continuous on the time scale of the experiment. Previous beam model studies, except for Ref. 9, have used time-independent beam equations.

Once $\gamma_p \Gamma_p$ is chosen to match the data at high power, the same value is used to calculate the transient current signal as a function of power, i.e., only the initial conditions are changed. As shown in Fig. 6 (solid line), the experimentally observed trend in POG signal amplitude with discharge power is not reproduced quantitatively although the correct trend is obtained.[20]

A typical calculated current waveform is shown in Fig. 9 for both a constant voltage boundary condition and a perturbed voltage boundary condition. Note that ringing

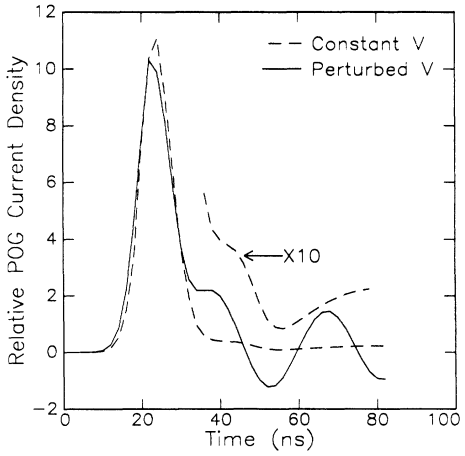

FIG. 9. Time-dependent current (POG signal) calculated using single-beam model with (dashed line) and without (solid lines) voltage perturbation. The POG current minus the steady-state current is expressed as a function of the steady-state current; the curve without voltage perturbation is magnified tenfold for longer times to illustrate the presence of ringing in the current waveform even when the voltage is held constant. Steady-state discharge conditions are 300 V, 0.49 mA cm^{-2}, and 0.037 W cm^{-3}. For times longer than the peak in the laser pulse intensity, the voltage perturbation is given by $V_{ss}[1+0.03e^{-t/\tau}\sin(\omega t)]$, where V_{ss} is the steady-state voltage, $\tau = 150$ ns, and $\omega/2\pi = 35$ MHz.

is observed in the calculated waveform even though the voltage is kept constant, albeit the magnitude is ~10 times smaller than that observed experimentally (Fig. 2). Nonetheless, the calculation shows that the ringing is inherent to the discharge and not entirely caused by the external circuit. Note that ringing is less evident in the companion paper because of the longer laser pulse duration employed there.

The physical interpretation of this ringing can be seen most easily from examination of the calculated plasma potential at the cathode and anode and the bulk electron flux across the discharge. In Fig. 10 the plasma potential is plotted for three different times during the photoemission experiment. As a result of the photoemission, the cathode sheath contracts slightly. Again, this is qualitatively consistent with the experimental data in Fig. 5 although the magnitude of the contraction is too small. The contraction is also observed directly from *in situ* electric field measurements in the following paper.[8] The cathode sheath contracts because the charge density has increased locally as a result of the avalanche. As the cathode contracts, bulk electrons diffuse behind the moving sheath edge (large negative current in middle plot of Fig. 11).

Near the anode, on the other hand, the plasma potential first decreases below the anode potential to allow excess negative charge to escape. This results in a rapid electron flux to the anode (Fig. 11). However, too much charge is extracted and the plasma potential subsequently increases above the initial value to constrain further electron loss. This overshoot in the plasma potential occurs *for fixed voltage across the gap* and is at least partially responsible for the observed current oscillations.

To evaluate the effects of nonconstant gap voltage, we add a damped oscillating potential to the voltage boundary condition. The form for this perturbation term is chosen to match experimental waveforms as shown in Fig. 3 (see caption to Fig. 9). Alternatively, we could have chosen to include a model for the external circuit but this would require the use of adjustable parameters for stray capacitance and inductance and would not provide additional insight. With the voltage perturbation term included, we find the magnitude of the initial current remains unchanged as a function of discharge power. However, the relative magnitude of the ringing is increased (Fig. 9) and is in better agreement with experimental observations (Fig. 2). Thus, we conclude that the external circuit is important in determining the magnitude of current oscillations, but their existence is inherent to the discharge's response to cathodic photoemission.

The quantitative inadequacies of the single-beam model imply that this approach does not properly account for the extent of avalanching in the sheath.[21] This is not surprising. Implicitly in the unidirectional assumption of the beam model is the neglect of all but forward angle scattering. This leads to a too-rapid traversal of the

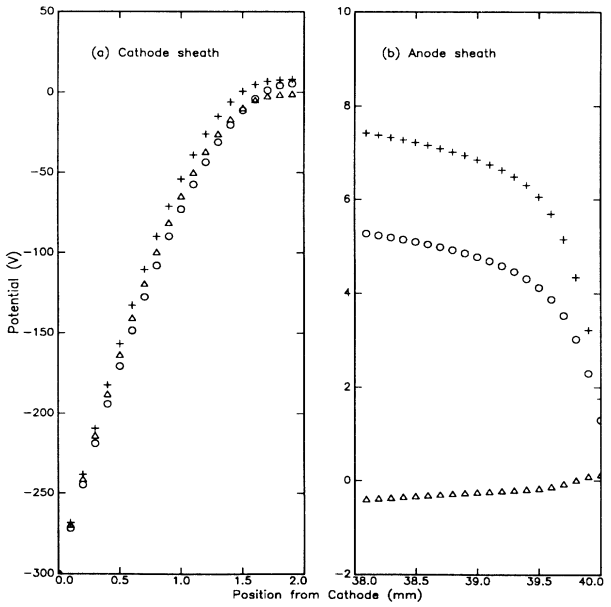

FIG. 10. Plasma potentials near (a) cathode and (b) anode for three different times during the photoemission experiment (ignoring voltage perturbation). The times are 0, 22, and 48 ns for ○'s, △'s, and +'s, respectively (see Fig. 9). Note the sheath contraction near the cathode and the change in sign and overshoot of the plasma potential near the anode. Steady-state discharge conditions are as given in Fig. 9.

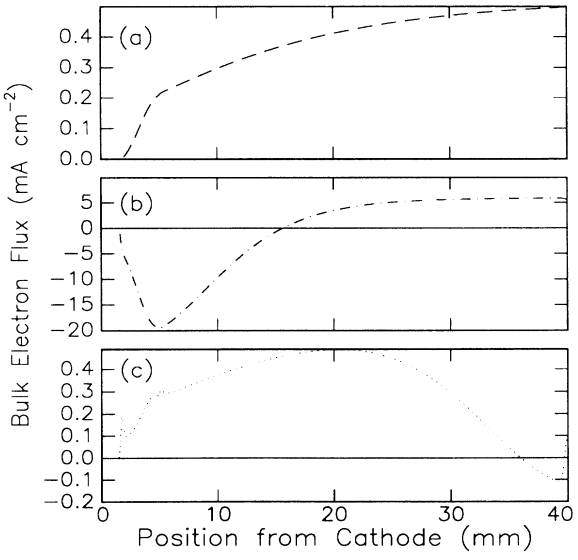

FIG. 11. Bulk electron flux (positive corresponds to electron flux toward the right and current toward the left) for three times during the photoemission experiment (ignoring voltage perturbation): (a) $t=0$, (b) $t=22$ ns, (c) $t=48$ ns. Note the large increase in bulk electron flux near the peak of the POG signal ($t=22$ ns). At this point, electrons move toward both the cathode fall because the sheath contracts and toward the anode because the field reverses. Discharge conditions as given in caption to Fig. 9.

sheath and a too-extensive penetration of the beam into the negative glow. Albeit with milder disagreement, similar conclusions were drawn when steady-state calculations of ion density and emission intensities were compared with experiment.[11,22,23] To model the avalanche accurately, it appears necessary to use hybrid particle-fluid or multibeam codes.[8,22,23]

E. POG signal dependence on discharge frequency

Another parameter that has a significant effect on the POG signal magnitude is discharge frequency (Fig. 6). As for dc discharges, the POG signal decreases when the rf power is increased. However, the magnitude of the POG signal for any given discharge power is smaller for a 250-kHz discharge than the dc discharge. This effect is observed when Al cathodes with a thin native oxide layer are irradiated at long wavelengths, near the photoelectric threshold. At shorter wavelengths, further from the photoelectric threshold, the difference in signals between rf and dc discharges is less apparent. Given this dependence on wavelength, one can rule out differences in discharge structure as being responsible for the difference in POG signal amplitude. Changes in surface properties must be responsible. Near threshold, positive charging of the oxide layer can substantially shift the photoelectric threshold to longer wavelengths by providing a strong local electric field to extract electrons near the surface.[24] For example, a surface charge density of only 5.5×10^{9} cm^{-2} is sufficient to produce an electric field of 10 kV/cm and a threshold shift on the order of 10 nm.[24] Thus, the photoelectric yield is enhanced in dc discharges relative to rf discharges where surface charging is periodically reduced.

IV. CONCLUSIONS

In this work we have investigated the effects that discharge power and frequency have on the avalanching of electrons created by photoemission at the cathode surface. Because of inherently higher gain, we find that both photoemission optogalvanic (POG) signals and transient optical emission intensities are enhanced by operating at lower discharge powers. The thicker sheath at lower power that results from lower charge density provides more extensive avalanching; the increase in sheath thickness more than compensates for the decrease in voltage across the sheath at low power. These conclusions are supported using single-beam and Monte Carlo simulations of the avalanches.

Modeling the effects of discharge power on POG signal magnitudes and transient emission spatial profiles using a single-beam, self-consistent model proved useful for generating qualitative insight. The model clearly shows that intense photoemission at the cathode lowers the plasma potential near the anode so that excess negative charge can escape. However, the potential overshoots in this adjustment and returns to steady state in an oscillatory fashion. Quantitative shortcomings of this model are attributed to the implicit assumption of forward-only scattering that leads to an underestimate of the degree of avalanching in the sheath and an insensitivity of the signals to changes in sheath thickness. Multibeam or hybrid particle-fluid codes appear necessary to accurately and self-consistently account for the observations reported.

The results obtained here indicate that intensification of discharges using photoelectron emission will be easier for lower-powered, thicker sheath discharges. Similarly, weaker discharges are most conducive to sensitive optogalvanic detection of photoemission from reactive surfaces.

We also observed a strong dependence of the POG signals on discharge frequency that is attributed to surface charging. For wavelengths close to threshold, the surface charge electric field shifts the photoelectric threshold to lower energy and thereby enhances the photoelectric yield. Thus, dc discharges show a stronger response than rf discharges under these conditions.

ACKNOWLEDGMENTS

We are grateful to J.-P. Boeuf for giving us his Monte Carlo computer code and for advising us on its use. We are also grateful to J.-P. Boeuf and S. W. Downey for stimulating discussions on electron avalanching and photoemission and to N. L. Schryer for advice concerning solutions of nonlinear partial differential equations We are most grateful for the fruitful collaboration and exchange of information with the authors of the following paper.

[1]J. J. Cuomo and C. R. Guarnieri, U.S. Patent No. 4,665,769 (1987); J. J. Cuomo, C. R. Guarnieri, and D. S. Yee, American Vacuum Society 35th National Symposium, Atlanta, Georgia, 1988, Abstract. No. PS-WeA9.

[2]S. W. Downey, A. Mitchell, and R. A. Gottscho, J. Appl. Phys. **63**, 5280 (1988); S. W. Downey, A. Mitchell, and R. A. Gottscho, Mater. Res. Soc. Symp. Proc. **117**, 1 (1988).

[3]G. S. Selwyn, B. D. Ai, and J. Singh, Appl. Phys. Lett. **52**, 1953 (1988).

[4]V. A. Godyak, *Soviet Radio Frequency Discharge Research*, Delphic Associates, Inc. (Falls Church, Virginia, 1986).

[5]H. A. Blevin, J. Fletcher, and L. M. Marzec, J. Phys. D **9**, 465 (1976); H. A. Blevin, J. Fletcher, S. R. Hunter, and L. M. Marzec, *ibid.* **9**, 471 (1976); H. A. Blevin, J. Fletcher, and S. R. Hunter, *ibid.* **11**, 2295 (1978); H. A. Blevin, J. Fletcher, and S. R. Hunter, *ibid.* **11**, 471 (1978).

[6]A. V. Phelps, International Conference on Ionization Phenomena in Gases, Swansea, 1987 (unpublished).

[7]C. E. Gaebe, T. R. Hayes, and R. A. Gottscho, Phys. Rev. A **35**, 2993 (1987).

[8]H. Debontride, J. Derouard, P. Edel, R. Romestain, N. Sadeghi, and J. P. Boeuf, following paper, Phys. Rev. A **40**, 5208 (1989).

[9]B. M. Jelenkovic and A. V. Phelps, Phys. Rev. A **36**, 5310 (1987); A. V. Phelps, B. M. Jelenkovic, and L. C. Pitchford, *ibid.* **36**, 5327 (1987).

[10]J. P. Boeuf and P. Segur, in *Interactions Plasma Froids Materiaux*, edited by C. Lejeune (Les Editions de Physique,

Paris, 1988), p. 113.
[11]R. A. Gottscho, A. Mitchell, G. R. Scheller, N. L. Schryer, D. B. Graves, and J. P. Boeuf, Electrochem. Soc. **88-22**, 1 (1988).
[12]J.-P. Boeuf and E. Marode, J. Phys. D **17**, 1133 (1984).
[13]R. A. Gottscho, R. H. Burton, D. L. Flamm, V. M. Donnelly, and G. P. Davis, J. Appl. Phys. **55**, 2707 (1984).
[14]G. P. Davis and R. A. Gottscho, J. Appl. Phys. **54**, 3080 (1983); G. R. Scheller, R. A. Gottscho, D. B. Graves, and T. Intrator, *ibid.* **64**, 598 (1988).
[15]R. A. Gottscho, G. P. Davis, and R. H. Burton, Plasma Chem. Plasma Proc. **3**, 193 (1983); J. Vac. Sci. Technol. A **1**, 622 (1983).
[16]M. L. Mandich, C. E. Gaebe, and R. A. Gottscho, J. Chem. Phys. **83**, 3349 (1985).
[17]S. R. Hunter and L. G. Christophororu, J. Chem. Phys. **80**, 6150 (1984); H. B. Milloy, R. W. Crompton, J. A. Rees, and A. G. Robertson, Aust. J. Phys. **30**, 61 (1977); G. N. Haddad and T. F. O'Malley, *ibid.* **35**, 35 (1982).
[18]J. Bretagne, G. Callede, M. Lepeutil, and V. Puech, J. Phys. D **19**, 761 (1986).
[19]D. Rapp and P. Englander-Golden, J. Chem. Phys. **43**, 1464 (1965).
[20]Note that the simulations could not be performed at lower discharge powers than indicated in Fig. 6 because of a numerical instability. At lower powers, the beam velocity can cross zero after the peak in the POG signal. This corresponds to beam reflection and even though it occurs when the beam density is negligible, the upwinded equations (Ref. 11) are ill suited to handle the velocity reversal. The decrease in the beam velocity at lower power is more severe than at higher power because of a stronger potential overshoot in the discharge response to intense photoemission.
[21]Another possible explanation for the problem with the beam model as applied here is that it assumes that both ions and bulk electrons respond instantaneously to changes in the local field. On the rapid time scale of these experiments, however, ion and electron inertia cannot be neglected. To account for these effects, we included two ordinary differential equations to solve for ion and bulk electron velocities. Following the approach of A. D. Richards, B. E. Thompson, and H. H. Sawin, Appl. Phys. Lett. **50**, 492 (1987), particle acceleration by the electic field is balanced with deceleration by collisions. Inclusion of these equations did not alter the calculated results significantly.
[22]M. Surendra and D. B. Graves, Bull. Am. Phys. Soc. **34**, 296 (1989).
[23]M. Surendra, D. B. Graves, and G. M. Jellum, Phys. Rev. A (to be published).
[24]E. O. Lawrence and L. B. Linford, Phys. Rev. **36**, 482 (1930).